

Joint 3D Object Detection and Tracking Using Spatio-Temporal Representation of Camera Image and LiDAR Point Clouds

Junho Koh^{1*}, Jaekyum Kim^{1*}, Jin Hyeok Yoo¹ Yecheol Kim¹ Dongsuk Kum² Jun Won Choi¹

¹Hanyang University

²Korea Advanced Institute of Science and Technology (KAIST)

{jhkoh, jkkim, jhyoo, yckim}@spa.hanyang.ac.kr, dskum@kaist.ac.kr, junwchoi@hanyang.ac.kr

Abstract

In this paper, we propose a new joint object detection and tracking (JoDT) framework for 3D object detection and tracking based on camera and LiDAR sensors. The proposed method, referred to as 3D DetecTrack, enables the detector and tracker to cooperate to generate a spatio-temporal representation of the camera and LiDAR data, with which 3D object detection and tracking are then performed. The detector constructs the spatio-temporal features via the weighted temporal aggregation of the spatial features obtained by the camera and LiDAR fusion. Then, the detector reconfigures the initial detection results using information from the tracklets maintained up to the previous time step. Based on the spatio-temporal features generated by the detector, the tracker associates the detected objects with previously tracked objects using a graph neural network (GNN). We devise a fully-connected GNN facilitated by a combination of rule-based edge pruning and attention-based edge gating, which exploits both spatial and temporal object contexts to improve tracking performance. The experiments conducted on both KITTI and nuScenes benchmarks demonstrate that the proposed 3D DetecTrack achieves significant improvements in both detection and tracking performances over baseline methods and achieves state-of-the-art performance among existing methods through collaboration between the detector and tracker.

Introduction

Multiple object tracking (MOT) based on sensor measurements (e.g., camera and LiDAR) is essential for machine perception tasks in robotics and autonomous driving applications. The traditional approach is the *tracking-by-detection* strategy, which detects objects based on a single snapshot of sensor measurements and temporally links the detection results over multiple snapshots. In this approach, detection and tracking are considered independent tasks and thus have been studied separately by different research communities.

Although the *tracking-by-detection* approach has been shown to be effective in numerous studies, the following question arises: *if our end goal is to identify moving objects based on the sequence of measurements received from the*

sensors, would it not be beneficial to jointly design and optimize both detectors and trackers to improve the performance of both?

Several works relevant to JoDT have been reported in the literature (Zhang et al. 2021; Wang et al. 2020; Wang, Kitani, and Weng 2020; Hu et al. 2019; Kim and Kim 2016; Kieritz, Hubner, and Arens 2018; Voigtlaender et al. 2019; Shenoj et al. 2020). The previous JoDT methods can be categorized into two approaches. The first approach integrates the re-identification network for object association into the detector and jointly optimizes them end-to-end. This approach was mostly developed for 2D MOT, including TrackRCNN (Voigtlaender et al. 2019), JDE (Wang et al. 2020), FairMOT (Zhang et al. 2021), RetinaTrack (Lu et al. 2020), and GSDT (Wang, Kitani, and Weng 2020). The second approach exploits the intermediate features extracted by the detector for MOT. The appearance cues and motion context identified by the detector were used to perform tracking. The 2D MOT methods in this category include MPNTrack (Brasó and Leal-Taixé 2020), RNN tracker (Kieritz, Hubner, and Arens 2018), CDT (Kim and Kim 2016), PredNet (Munjul et al. 2020), and Chained-Tracker (Peng et al. 2020). The JoDT methods for 3D MOT include the mono3DT (Hu et al. 2019) and JRMOT (Shenoj et al. 2020).

In this paper, we propose a new JoDT method, referred to as *3D DetecTrack*, which performs 3D MOT based on the sequence of the camera images in conjunction with LiDAR point clouds. In our framework, the detector and tracker cooperate to utilize spatio-temporal information to perform 3D object detection and tracking.

First, the detector generates spatio-temporal features by combining the spatial features produced by the camera and LiDAR sensor fusion over time. This operation creates features for detecting objects with higher accuracy. The detection step in 3D DetecTrack also exploits the *tracklet* maintained by the tracker to improve detection accuracy. The region proposal network (RPN) calibrates an objectness score based on the intersection of union (IoU) between the anchor box and its nearest tracklet box. Then, refinement network aggregates the instance-level features from adjacent frames and adjusts the classification scores in a manner similar to RPN. This design is inspired by the intuition that the tracklets provide useful cues, which can increase the confidence score for detecting objects.

*These authors contributed equally.

Next, the tracking step in 3D DetecTrack utilizes the spatio-temporal features generated by the detector in the object association task. According to the 3D bounding boxes provided by the detector, the tracker pools the object features from the temporally aggregated features and point-encoded features. Then, it associates the detected objects with those in the tracklet through a graph neural network (GNN). We consider a fully-connected GNN model to represent both spatial and temporal relations between the objects. However, this approach causes the connections in the graph to become excessively dense, which makes the convergence of the GNN slower. To address this issue, we employ both rule-based edge pruning and attention-based edge gating. Rule-based edge pruning removes the edges of a graph based on the distance between the objects comprising a pair. Attention-based edge gating learns to weight the edges of the graph depending on the input. Attending to only the critical edges of the graph enables the GNN to operate faster and more accurate. The detector and tracker are trained in an end-to-end fashion and the loss terms related to both tasks are minimized simultaneously. The contributions of this paper are summarized as follows

- We propose a novel JoDT method in which the detector and tracker can collaborate to obtain the spatio-temporal representation of multi-sensor data for 3D MOT.
- We design a cooperative JoDT model that reconfigures the outputs of both the RPN and the refinement network based on the information inferred from the tracked objects and also utilizes the spatio-temporal features formed by the detector for object association.
- We devise a spatio-temporal gated GNN (SG-GNN), which adopts both rule-based pruning and attention-based edge gating to improve the tracking performance.
- We evaluate the performance of the proposed 3D DetecTrack on both the KITTI and nuScenes datasets. Our experiments demonstrate that the proposed 3D DetecTrack achieves dramatic performance improvements over the baselines and outperforms existing 3D MOT methods on both datasets.

Related Work

3D Object Detection and Multi Object Tracking

3D object detection methods can be divided into two categories: (i) LiDAR-only and (ii) sensor fusion-based methods. The LiDAR-only 3D detectors encode point clouds using the PointNet (Qi et al. 2017a,b) and detect objects by applying a detection-head network. These methods include PointRCNN (Shi, Wang, and Li 2019), Part A² (Shi et al. 2019), STD (Yang et al. 2019), 3DSSD (Yang et al. 2020), VoxelNet (Zhou and Tuzel 2018), SECOND (Yan, Mao, and Li 2018), PointPillar (Lang et al. 2019), and CIASSD (Zheng et al. 2021). To overcome the limitations of the LiDAR-only approach, many sensor fusion-based 3D object detection methods have been developed, which enhance object features by combining intermediate features obtained from the camera image and LiDAR point clouds. These methods include ContFuse (Liang et al. 2018), MMF

(Liang et al. 2019), CLOCs (Pang, Morris, and Radha 2020), and 3D-CVF (Yoo et al. 2020). In our method, we adopt a 3D-CVF (Yoo et al. 2020) as the baseline detector.

Numerous 3D MOT methods follow the *tracking-by-detection* paradigm (Weng et al. 2020a; Chiu et al. 2020; Weng et al. 2020b; Zhai et al. 2020; Zhang et al. 2019; Baser et al. 2019), in which the objects are first detected in 3D, the tracker then associates the detected objects. Since a simple but effective baseline 3D MOT method, AB3DMOT was proposed in (Weng et al. 2020a). Various 3D MOT methods have been proposed including mmMOT (Zhang et al. 2019), FANTrack (Baser et al. 2019), and GNN3DMOT (Weng et al. 2020b). These methods do not consider the co-optimization of detection and tracking, limiting their potential for further performance gains.

Joint Object Detection and Tracking

Various JoDT methods have been proposed in (Zhang et al. 2021; Wang et al. 2020; Wang, Kitani, and Weng 2020; Peng et al. 2020; Hu et al. 2019; Shenoi et al. 2020; Kim and Kim 2016; Kieritz, Hubner, and Arens 2018; Ke et al. 2019; Munjal et al. 2020). In the early phase, the idea of JoDT was adopted for 2D MOT. CDT (Kim and Kim 2016) restored undetected objects by examining forward and backward tracing of tracking results. JDE (Wang et al. 2020) and FairMOT (Zhang et al. 2021) incorporated a re-identification model of the tracker into the detector. GSDT (Wang, Kitani, and Weng 2020) performed simultaneous object detection and tracking using GNN.

Recently, JoDT has been extended to 3D MOT. Mono3DT (Hu et al. 2019) enhanced the performance of monocular camera-based 3D object detection by tracking moving objects across frames via occlusion-aware association and depth-ordering matching. JRMOT (Shenoi et al. 2020) combined re-identification, detection and tracking steps into a joint probabilistic data association framework. The proposed 3D DetecTrack differs from the aforementioned methods in that the detector and the tracker cooperatively generate strong spatio-temporal features, which are then used to perform 3D object detection and tracking.

Proposed Method

In this section, we present the details of the proposed 3D *DetecTrack* method.

Overview

The overall architecture of the proposed 3D DetecTrack is depicted in Figure 1. The proposed JoDT consists of i) detection stage and ii) tracking stage. We denote the tracklet at the $(t - 1)$ th time step as $T_{t-1} = (T_{t-1,1}, \dots, T_{t-1,N_T})$, where N_T is the number of tracked objects. The objective of JoDT is to produce the detection results $\mathcal{D}_t = (\mathcal{D}_{t,1}, \dots, \mathcal{D}_{t,N_D})$ and the tracklet T_t given T_{t-1} and the sensor measurements Y_t acquired at the t th time step, where N_D is the number of detected objects. Note that N_T and N_D can vary over time.

Detection stage: We adopt the two-stage detection model, 3D-CVF (Yoo et al. 2020) as our baseline 3D object

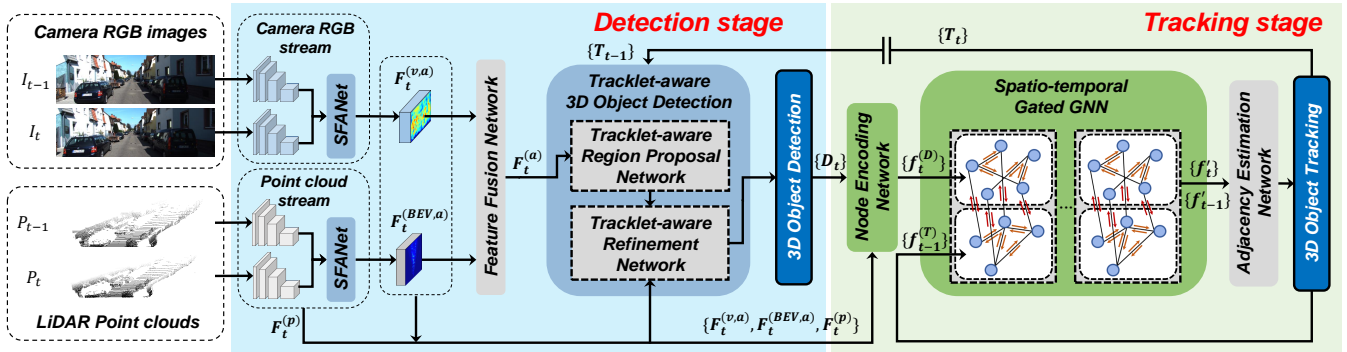


Figure 1: **Overall architecture of the proposed 3D DetecTrack:** 3D DetecTrack effectively utilizes the spatio-temporal information to perform JoDT. The camera and LiDAR features are temporally aggregated via SFANet. Trk-RPN and Trk-RefNet reconfigure the detection output using the tracklet from the tracker. Using the RoI-aligned features produced by the detector, the objects are associated using SG-GNN. SG-GNN exploits spatio-temporal relations among objects to perform object association. Finally, the affinity matrix is calculated based on the output of SG-GNN. Our proposed network is trained in an end-to-end manner.

detector. We choose the 3D-CVF because it can generate both camera-view 2D features and bird’s eye view (BEV) LiDAR features. In our work, we modify the 3D-CVF to produce spatio-temporal features. Let $(F_{t-1}^{(v)}, F_t^{(v)})$ be the camera-view features extracted from the images (I_{t-1}, I_t) via the shared CNN backbone network. Similarly, let $(F_{t-1}^{(BEV)}, F_t^{(BEV)})$ be the BEV features obtained by the voxelization process followed by the 3D CNN. The *spatio-temporal feature aggregation network (SFANet)* aggregates two concatenated features $(F_{t-1}^{(v)}, F_{t-1}^{(BEV)})$ and $(F_t^{(v)}, F_t^{(BEV)})$ to produce the spatio-temporal features $(F_t^{(v,a)}, F_t^{(BEV,a)})$. Because these two features are temporally correlated but not exactly identical, they should be combined in different proportions, depending on their relevance to the end task. For this goal, we employ a *gated attention mechanism*, which adaptively balances the contributions of $(F_{t-1}^{(v)}, F_{t-1}^{(BEV)})$ and $(F_t^{(v)}, F_t^{(BEV)})$ by multiplying the learnable weight maps A_{t-1} and A_t . This operation will be described in detail later. The detector then fuses the camera features $F_t^{(v,a)}$ and LiDAR features $F_t^{(BEV,a)}$ into $F_t^{(a)}$, following the procedure of 3D-CVF (Yoo et al. 2020).

Based on the features $F_t^{(a)}$ produced by SFANet, the RPN predicts the object box and objectness scores for each anchor box. Subsequently, the refinement stage refines the box coordinates and computes the classification scores. Our 3D DetecTrack enhances the RPN and refinement stages by utilizing the information obtained from the tracklet T_{t-1} . The Trk-RPN calibrates the objectness score based on the IoU between each anchor and its nearest tracklet in the BEV domain. The objects maintained in the tracklet are supposed to increase the likelihood of objects being detected in the vicinity, which implies that the tracker assists with the detection task. The Trk-RefNet aggregates the instance-level features at time t and $t-1$ based on the cosine similarity-based attention and adjusts the classification score based on IoU between the anchor and the nearest tracklet.

Tracking stage: The tracking stage associates the detection results \mathcal{D}_t with the tracklet T_{t-1} based on the spatio-temporal features obtained in the detection stage. The 3D boxes for the detected objects in \mathcal{D}_t are projected into the BEV domain to produce 2D boxes. Then, 2D RoI pooling is performed for the i th object to extract the RoI-aligned features, $f_{t,i}^{(v,a)}$ and $f_{t,i}^{(BEV,a)}$ from $F_t^{(v,a)}$ and $F_t^{(BEV,a)}$, respectively. In addition, the tracker pools the point-encoded features $f_{t,i}^{(p)}$ via 3D-RoI alignment method proposed in (Yoo et al. 2020). These features are concatenated as $f_{t,i}^{(D)} = (f_{t,i}^{(v,a)}, f_{t,i}^{(BEV,a)}, f_{t,i}^{(p)})$. Similarly, a similar feature pooling procedure is applied for the i th object in the tracklet T_{t-1} . This yields the concatenated features $f_{t-1,i}^{(T)} = (f_{t-1,i}^{(v,a)}, f_{t-1,i}^{(BEV,a)}, f_{t-1,i}^{(p)})$. Two feature groups $f_{t,i}^{(D)}$ and $f_{t-1,i}^{(T)}$ serve for the discriminative features used for object association.

Two features $(f_{t,1}^{(D)}, \dots, f_{t,N_D}^{(D)})$ and $(f_{t-1,1}^{(T)}, \dots, f_{t-1,N_T}^{(T)})$ are fed into the SG-GNN. These features are represented by nodes in the graph. The SG-GNN associates the objects in \mathcal{D}_t with those in T_{t-1} by matching $(f_{t,1}^{(D)}, \dots, f_{t,N_D}^{(D)})$ and $(f_{t-1,1}^{(T)}, \dots, f_{t-1,N_T}^{(T)})$. We consider a fully connected graph to model the spatial and temporal relations among the objects in \mathcal{D}_t and T_{t-1} . Because these dense connections can lead to unnecessary feature exchanges between nodes, we devise rule-based pruning and attention-based edge gating to improve SG-GNN. Finally, the SG-GNN produces an affinity matrix based on the pairwise association score for all edges connecting the nodes from \mathcal{D}_t and those from T_{t-1} . The affinity matrix is then processed by the Hungarian algorithm (Kuhn 1955) to output the final tracklet T_t . The entire procedure is repeated until the input sequence is complete.

Spatio-Temporal Feature Aggregation Network

The SFANet selectively combines two spatial feature maps obtained in two adjacent time steps.

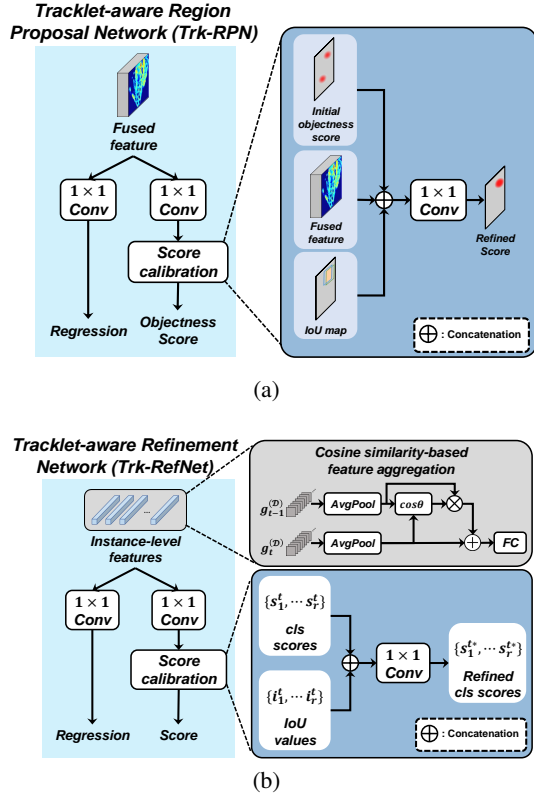


Figure 2: Structure of (a) Tracklet-aware Region Proposal Network (Trk-RPN) and (b) Tracklet-aware Refinement Network (Trk-RefNet): Both Trk-RPN and Trk-RefNet utilize the tracklet T_{t-1} to improve the detection performance.

Suppose that there exist two feature maps $F_{t-1}^{(\cdot)}$ and $F_t^{(\cdot)}$ of the same size $C \times X \times Y$. The SFANet applies the weighted aggregation of $F_{t-1}^{(\cdot)}$ and $F_t^{(\cdot)}$ as

$$F_t^{(\cdot,a)} = A_t \otimes F_t^{(\cdot)} + A_{t-1} \otimes F_{t-1}^{(\cdot)}, \quad (1)$$

where \otimes denotes pixel-wise multiplication and the attention maps A_t and A_{t-1} have a size of $1 \times X \times Y$. The attention maps A_t and A_{t-1} are computed as

$$A_t = \sigma(\text{conv}_{3 \times 3}(F_t^{(\cdot)} \oplus F_{t-1}^{(\cdot)})) \quad (2)$$

$$A_{t-1} = 1 - A_t \quad (3)$$

where $\sigma(\cdot)$ is the logistic-sigmoid function, $\text{conv}_{3 \times 3}$ are the convolutional layers with 3×3 kernels, and the operation \oplus denotes concatenation.

Tracklet-aware 3D Object Detection

The detailed structures of Trk-RPN and Trk-RefNet are depicted in Figure 2 (a) and (b), respectively.

Trk-RPN: Trk-RPN produces P region proposals $\mathcal{R}_1, \dots, \mathcal{R}_P$ based on the feature maps $F_t^{(a)}$ obtained by the SFANet. For each anchor, the initial objectness score and 3D

box coordinates are predicted through a 1×1 convolution. The objectness score is calibrated using the IoU between the anchor box and tracklet boxes in T_{t-1} in BEV domain. For each anchor, IoU is obtained as the highest IoU among all tracklet boxes. IoU is set to 0 if the anchor does not overlap with any tracklet box. The input feature, initial objectness score, and IoU are concatenated and passed through the additional feedforward neural network to output the adjusted objectness score. Because higher IoU values indicate a higher chance of an anchor being positive, they are expected to increase the objectness score of the anchor.

Trk-RefNet: Trk-RefNet refines the 3D box prediction and classification score for all region proposals found by Trk-RPN. Based on the j th region proposal \mathcal{R}_j , the RoI-aligned features $g_{t,j}^{(v,a)}$ and $g_{t,j}^{(BEV,a)}$ are pooled from $F_t^{(v,a)}$ and $F_t^{(BEV,a)}$. In addition, 3D-RoI alignment (Yoo et al. 2020) is applied to extract the point-encoded features $g_{t,j}^{(p)}$. These features are concatenated as $g_{t,j}^{(D)} = (g_{t,j}^{(v,a)}, g_{t,j}^{(BEV,a)}, g_{t,j}^{(p)})$. Whereas SFANet combines feature maps without any alignment, Trk-RefNet spatially aligns object features before performing feature aggregation. Treating \mathcal{R}_j as an anchor, Trk-RPN predicts the 3D bounding box for the $(t-1)$ th time step based on $F_{t-1}^{(a)}$. Then, the concatenated features for the $(t-1)$ th time step are obtained as $g_{t-1,j}^{(D)} = (g_{t-1,j}^{(v,a)}, g_{t-1,j}^{(BEV,a)}, g_{t-1,j}^{(p)})$. Finally, the instance-level features, $g_{t,j}^{(D)}$ and $g_{t-1,j}^{(D)}$ are aggregated as

$$h_{t,j} = g_{t,j}^{(D)} + w(g_{t,j}^{(D)}, g_{t-1,j}^{(D)})g_{t-1,j}^{(D)}, \quad (4)$$

$w(g_{t,j}^{(D)}, g_{t-1,j}^{(D)})$ denotes the cosine similarity defined as

$$w(g_{t,j}^{(D)}, g_{t-1,j}^{(D)}) = \frac{\phi(g_{t,j}^{(D)}) \odot \phi(g_{t-1,j}^{(D)})}{\|\phi(g_{t,j}^{(D)})\|_2 \|\phi(g_{t-1,j}^{(D)})\|_2}, \quad (5)$$

where $\phi(\cdot)$ denotes the global average pooling operation, and \odot denotes the inner product operation. The cosine similarity measures the correlation between two detection results and is used to adjust the weight applied to the features at the $(t-1)$ th time step.

Trk-RefNet calibrates the classification score by applying the fully-connected layers to the initial classification score concatenated with the IoU between the region proposal and the nearest tracklet box.

Spatio-Temporal Gated Graph Neural Network

Spatio-temporal graph: The graph models the relation among the objects in \mathcal{D}_t and T_{t-1} . According to the 3D boxes in \mathcal{D}_t and T_{t-1} , RoI pooling is performed to obtain the RoI-aligned features $(f_{t,1}^{(D)}, \dots, f_{t,N_D}^{(D)})$ and $(f_{t-1,1}^{(T)}, \dots, f_{t-1,N_T}^{(T)})$. These RoI-aligned features are represented by nodes, and their explicit pairwise relationships are encoded by the edges. Previous works (Weng et al. 2020b; Wang, Kitani, and Weng 2020) used a GNN connecting the nodes at the t th time step with those at the $(t-1)$ th time step. In our work, we consider a spatio-temporal graph, which additionally connects the nodes within the nodes at the t th time

step as well as those within the nodes at the $(t - 1)$ th time step. This captures the spatial relation between the objects. Our fully-connected graph is motivated by the idea that understanding the spatial relation between objects will help better associate the objects temporally. However, owing to the dense connections of the graph, a GNN may require unnecessary exchanges of the features, thereby leading to a higher convergence speed. To address this issue, we apply rule-based edge pruning and attention-based edge gating to SG-GNN, as described below.

Rule-based edge pruning: Rule-based edge pruning discards unnecessary edges from a graph based on the spatial distance between objects. Two types of rules are applied. First, the edges connecting the nodes at the t th time step are pruned if the Euclidean distance between the object centers in the BEV domain is larger than the threshold L_s meter. Similarly, the edges connecting the nodes at the $(t - 1)$ th time step are pruned according to the same condition. This implies that the SG-GNN only attends to the spatial relation between nearby objects. Second, the edges connecting the nodes between the t th time step and the $(t - 1)$ th time step are pruned if the Euclidean distance between objects is larger than L_t meter. This design is justified by the fact that objects that are distant from each other are less likely to be associated. These pruning rules can simplify the node connectivity, thereby requiring much fewer iterations. In our experiments, we set $L_s = 15$ meter and $L_t = 5$ meter based on an empirical study.

Attention-based edge gating: We also apply attention-based edge gating, in which an *attention mechanism* is used to attend the model only on the influential edges. This method adaptively adjusts the weight for the edge based on the similarity of the two features associated with the nodes at both ends. The basic node feature aggregation step follows the rule suggested in (Morris et al. 2019). Consider N source nodes $n_{A,1}, \dots, n_{A,N}$ and a single target node n_B . In the intermediate iteration of GNN, we have the features $f_{A,1}, \dots, f_{A,N}$ and f_B at the nodes $n_{A,1}, \dots, n_{A,N}$ and n_B , respectively. The attention weight a_i is applied to the directed edge $E_{n_{A,i} \rightarrow n_B}$ from $n_{A,i}$ to n_B during node feature aggregation. Specifically, a_i is multiplied by the features $f_{A,i}$ when aggregating the features $f_{A,1}, \dots, f_{A,N}$ at node n_B . The attention weight a_i is calculated by

$$s_k = \frac{f_{A,k} \circ f_B}{\|f_{A,k}\|_2 \|f_B\|_2} \quad (6)$$

$$a_i = \frac{e^{w \cdot s_i}}{\sum_{k=1}^N e^{w \cdot s_k}} \quad (7)$$

where \circ denotes the dot product, and w is the learnable parameter. This attention weight reduces the influence of edges in which the two features are not aligned well. This enables the SG-GNN to focus only on the association of important features.

Object Association

After a fixed number of iterations, the SG-GNN ends up with the features $(f'_{t,1}, \dots, f'_{t,N_D})$ and $(f'_{t-1,1}, \dots, f'_{t-1,N_T})$ at the nodes. The affinity matrix A is constructed based on the

association score between the objects in \mathcal{D}_t and those in T_{t-1} . The (i, j) th element of A is provided by the association score A_{ij} between $f'_{t-1,i}$ and $f'_{t,j}$, which is calculated by

$$A_{ij} = \sigma(\text{fc}(f'_{t-1,i} \otimes f'_{t,j})) \quad (8)$$

where fc represents fully connected layers with a depth of 3. The association score has a value between 0 and 1 and the affinity matrix A is fed to the Hungarian algorithm (Kuhn 1955) to determine the tracklet T_t .

Loss Function

We adopt a multi-task loss to train the 3D DetecTrack. The total loss function comprises the detection loss L_{det} and tracking loss L_{trk} , i.e., $L_{\text{total}} = L_{\text{det}} + L_{\text{trk}}$. The detection loss L_{det} is expressed as

$$L_{\text{det}} = L_{\text{rpn}} + L_{\text{ref}} \quad (9)$$

where L_{rpn} denotes the RPN loss used to train the network pipeline up to Trk-RPN, and L_{ref} denotes the refinement loss in training Trk-RefNet. Following the setup in (Yoo et al. 2020), the RPN loss L_{rpn} comprises the focal loss (Lin et al. 2017) for the classification task and the Smoothed-L1 loss for the regression task. The refinement loss L_{ref} is defined similarly.

The tracking loss L_{trk} measures the mean squared error (MSE) of the affinity matrix A , defined as

$$L_{\text{trk}} = \frac{1}{N_D \cdot N_T} \sum_{i=1}^{N_T} \sum_{j=1}^{N_D} (A_{ij} - A_{ij}^{gt})^2. \quad (10)$$

Note that A^{gt} represents the ground truth (GT) of the affinity matrix A . The GT affinity matrix A^{gt} is calculated in two steps. In the first step, the 3D IoU between the output D_t and its GT boxes is calculated and the object ID of the GT box is assigned to the object in D_t if the highest 3D IoU is above 0.5. Comparing the object IDs in T_{t-1} and those assigned to D_t , we assign 0 or 1 to the GT affinity matrix A^{gt} . In the training phase, our 3D DetecTrack model regards the GT for D_{t-1} as the tracklet T_{t-1} .

Experiments

KITTI dataset

Dataset and evaluation metrics: The KITTI dataset was collected from urban driving scenarios using a single Point-grey camera and Velodyne HDL-64E LiDAR (Geiger, Lenz, and Urtasun 2012). To validate our method, we split the tracking training dataset evenly into *train* set and *valid* set by half, following (Weng et al. 2020b). Because the KITTI object detection dataset did not contain sequence data, performance was evaluated only on the KITTI object tracking dataset. As a benchmark, we evaluated the 3D MOT performance on the KITTI object tracking *valid* dataset. As 3D MOT performance metrics, we used sAMOTA, AMOTA, and AMOTP metrics (Weng et al. 2020a) as well as the standard CLEAR metric (Bernardin and Stiefelhagen 2008). We also examine the 2D MOT performance on the KITTI object tracking *test* dataset for the *Car* category. For 2D MOT,

| Method | Input Data | Runtime (ms) | sAMOTA (%) | AMOTA (%) | AMOTP (%) | MOTA (%) | MOTP (%) |
|--|------------|--------------|--------------|--------------|--------------|--------------|--------------|
| FlowMOT (Zhai et al. 2020) | 3D | - | 90.56 | 43.51 | 76.08 | 85.13 | 79.37 |
| AB3DMOT (Weng et al. 2020a) | 3D | 4.7 | 93.28 | 45.43 | 77.41 | 86.24 | 78.43 |
| mmMOT (Zhang et al. 2019) | 2D + 3D | 20 | 70.61 | 33.08 | 72.45 | 74.07 | 78.16 |
| FANTrack (Baser et al. 2019) | 2D + 3D | 70 | 82.97 | 40.03 | 75.01 | 74.30 | 75.24 |
| GNN3DMOT (Weng et al. 2020b) | 2D + 3D | - | 93.68 | 45.27 | 78.10 | 84.70 | 79.03 |
| Method of (Weng, Yuan, and Kitani 2020) | 2D + 3D | - | 92.37 | 44.96 | 76.83 | 84.49 | 78.32 |
| PC-TCNN (Wu et al. 2021) | 3D | - | 95.44 | 47.64 | - | - | - |
| 3D-CVF (Yoo et al. 2020) + mmMOT (Zhang et al. 2019) | 2D + 3D | 20 | 75.22 | 35.50 | 78.06 | 75.62 | 79.73 |
| 3D-CVF (Yoo et al. 2020) + AB3DMOT (Weng et al. 2020a) | 2D + 3D | 4.7 | 93.85 | 46.47 | 79.64 | 88.83 | 80.11 |
| Proposed method | 2D + 3D | 160 (37) | 96.49 | 48.87 | 81.56 | 91.46 | 82.24 |

Table 1: **3D MOT performance on KITTI tracking *valid* set for *Car* class:** The number in parentheses indicates the runtime for the tracking stage only.

| Method | mAP | sAMOTA (%) | AMOTA (%) | AMOTP (%) | MOTA (%) | MOTP (%) |
|---|--------------|--------------|--------------|--------------|--------------|--------------|
| FANTrack (Baser et al. 2019) | - | 19.64 | 2.36 | 22.92 | 18.60 | 39.82 |
| mmMOT (Zhang et al. 2019) | - | 23.93 | 2.11 | 21.28 | 19.82 | 40.93 |
| GNN3DMOT (Weng et al. 2020b) | - | 29.84 | 6.21 | 24.02 | 23.53 | 46.91 |
| AB3DMOT (Weng et al. 2020a) | - | 39.90 | 8.94 | 29.67 | 31.40 | 57.54 |
| Method of (Weng, Yuan, and Kitani 2020) | - | 28.96 | 11.36 | 25.83 | 22.81 | 41.99 |
| Baseline | 49.15 | 39.48 | 8.99 | 24.17 | 36.91 | 54.20 |
| Proposed method | 52.89 | 45.60 | 11.43 | 27.69 | 43.49 | 55.57 |

Table 2: **3D MOT performance on nuScenes validation set**

we used the KITTI evaluation metric (Luiten et al. 2020) including HOTA, DetA, and AssA. Because our method was designed under the JoDT framework, we also evaluated the 3D detection performance. As a performance metric, we used the average precision (AP) with three difficulty levels, i.e., "easy", "moderate", and "hard" as suggested in (Geiger, Lenz, and Urtasun 2012).

Implementation details: Our 3D DetecTrack model was trained in two steps. In the first step, we trained only the detection stage of the 3D DetecTrack using both the KITTI object detection and tracking datasets. The detection stage requires tracklet T_{t-1} for training. Since the detection dataset does not contain sequence data, the sequence was created by copying the same data. We trained the detection stage following the setup suggested in (Yoo et al. 2020). In the second step, the detection stage was initialized with the pre-trained model and the entire 3D DetecTrack model was trained end-to-end on the KITTI object tracking dataset. We trained the entire network over 40 epochs using the ADAM optimizer (Kingma and Ba 2014). The initial learning rate was set to 10^{-4} and decayed by a factor of 0.1 at the 26th and 35th epochs. The weight decay parameter was set to 10^{-4} , and the mini-batch size was set to 4.

nuScenes dataset

Dataset and evaluation metrics: The nuScenes dataset is a large scale autonomous driving dataset which contains more than 1,000 driving scenarios. The dataset was collected using six multi-view cameras, 32-channel LiDAR, and 360-degree object annotations. We evaluated 3D MOT performance for 7 categories (bicycle, bus, car, motorcycle, pedestrian, trailer and truck), as a subset of the detection categories in (Caesar et al. 2020). We also evaluated the 3D detection performance for 10 categories, including barrier, construction vehicle, and traffic cone as well as the aforementioned 7 categories. As 3D MOT performance metrics, we used the standard CLEAR metric (Bernardin and Stiefelhagen 2008) and the sAMOTA, AMOTA, and AMOTP met-

rics (Weng et al. 2020a). We used the nuScenes detection score (NDS) (Caesar et al. 2020) as a 3D detection performance metric.

Implementation details: We trained the 3D DetecTrack using a similar procedure similar to that used for the KITTI benchmark. We trained the entire model over 20 epochs. The initial learning rate was set to 10^{-4} and decayed by a factor of 0.1 at the 13th and 17th epochs. The rest of configurations were the same as those for KITTI.

Experimental Results

Performance on KITTI: Table 1 presents the 3D MOT performance and runtime evaluated on the KITTI tracking *valid* set. The KITTI benchmark provides a test dataset for 2D MOT, but not for 3D MOT; therefore, we strictly followed the 3D MOT evaluation procedure presented in (Weng et al. 2020a). We compared our 3D DetecTrack with several outstanding 3D MOT methods including FlowMOT (Zhai et al. 2020), AB3DMOT (Weng et al. 2020a), mmMOT (Zhang et al. 2019), FANTrack (Baser et al. 2019), GNN3DMOT (Weng et al. 2020b), the method of (Weng, Yuan, and Kitani 2020), and PC-TCNN (Wu et al. 2021). These 3D MOT methods adopt different 3D detectors. Thus, as shown in Table 1, we also evaluate the performance of mmMOT (Zhang et al. 2019) and AB3DMOT (Weng et al. 2020a) combined with the vanilla 3D-CVF to compare the ability of the trackers only. Table 1 shows that the proposed method outperforms the existing 3D MOT methods by a significant margin for all MOT metrics considered. In particular, our 3D DetecTrack performs better than the current state-of-the-art method, PC-TCNN. The proposed 3D DetecTrack also achieves better performance than AB3DMOT (Weng et al. 2020a) and mmMOT (Zhang et al. 2019) when 3D-CVF is used as a 3D detector.

We also evaluate the 2D MOT performance on the KITTI object tracking *test* set (refer to the official evaluation benchmark on the KITTI leaderboard). Due to space concerns, we provide the 2D MOT performance in the Appendix. 2D

| | SG-GNN | Trk-RPN | Trk-RefNet | SFANet | AP_{easy} | $AP_{mod.}$ | AP_{hard} | sAMOTA (%) | AMOTA (%) | AMOTP (%) |
|----------|--------|---------|------------|--------|--------------|--------------|--------------|--------------|--------------|--------------|
| Baseline | | | | | 90.32 | 89.37 | 88.89 | 92.15 | 45.23 | 77.46 |
| Ours | ✓ | | | | 90.32 | 89.37 | 88.89 | 94.97 | 47.93 | 80.48 |
| | ✓ | ✓ | | | 97.56 | 89.96 | 89.35 | 95.56 | 48.34 | 80.89 |
| | ✓ | ✓ | ✓ | | 98.41 | 90.32 | 90.08 | 96.02 | 48.56 | 81.16 |
| | ✓ | ✓ | ✓ | ✓ | 99.27 | 91.01 | 90.83 | 96.49 | 48.87 | 81.56 |

Table 3: **Ablation study for evaluating SFANet and tracklet-aware 3D object detection:** The ablation study is conducted on KITTI *valid* set for *Car* class.

| | SFANet + Trk-RPN + Trk-RefNet | Rule-based edge-pruning | Attention-based edge gating | Runtime (ms) | sAMOTA (%) | AMOTA (%) | AMOTP (%) | MOTA (%) | MOTP (%) |
|----------|----------------------------------|----------------------------|--------------------------------|--------------|--------------|--------------|--------------|--------------|--------------|
| Baseline | | | | - | 92.15 | 45.23 | 77.46 | 86.72 | 79.52 |
| Ours | ✓ | | | 41 | 94.02 | 46.79 | 78.81 | 88.45 | 79.99 |
| | ✓ | ✓ | | 34 | 95.50 | 48.04 | 81.03 | 90.21 | 81.98 |
| | ✓ | ✓ | | 37 | 96.49 | 48.87 | 81.56 | 91.46 | 82.24 |
| | | | ✓ | | | | | | |

Table 4: **Ablation study for evaluating rule-based edge-pruning and attention-based edge gating:** The ablation study is conducted on KITTI *valid* set for *Car* class.

MOT results are obtained by projecting 3D bounding boxes to the camera domain and generating 2D bounding boxes enclosing the projected coordinates. Although the proposed 3D DetecTrack is not originally designed for 2D MOT task, it achieves comparable performance to that of the current state-of-the-art 2D MOT methods. Note that the runtime of the tracker in the proposed method (37ms) is comparable to that of the existing tracking methods.

Performance on nuScenes: Table 2 presents the 3D MOT performance on nuScenes validation set. The baseline algorithm uses the original 3D-CVF and the vanilla fully-connected GNN. The proposed approach improves on the baseline by 3.74% in mAP and 6.12%, 2.44% and 3.52% in sAMOTA, AMOTA, and AMOTP, respectively. The 3D DetecTrack achieves the best performance among the candidates in the sAMOTA, AMOTA, and MOTA metrics. The per-class performance on both 3D detection and MOT tasks is provided in the Appendix. This shows that the proposed method achieves a particularly remarkable performance gain on bicycle, motorcycle, bus, and truck categories.

Ablation Study

In this section, we present an ablation study conducted to validate the contributions of the proposed design to our 3D DetecTrack. Experiments were conducted on the KITTI *valid* set. Our baseline was chosen as a combination of the original 3D-CVF and the baseline GNN. Table 3 presents how much the components of the 3D DetecTrack, SG-GNN, SFANet, Trk-RPN, and Trk-RefNet improve the performance on both 3D detection and MOT tasks. When the SG-GNN is added to the baseline, both temporal and spatial object context is exploited for object association, improving the sAMOTA performance by 2.82%. Both Trk-RPN and Trk-RefNet improve both the detection and MOT performance by utilizing the information from the tracklets. Trk-RPN yields a 0.59% gain in $AP_{mod.}$ detection performance and a 0.59% gain in sAMOTA MOT performance. Trk-RefNet achieves a 0.36% gain in $AP_{mod.}$ and a 0.46% gain in sAMOTA. Totally, both Trk-RPN and Trk-RefNet achieve 0.95% and 1.05% gains in $AP_{mod.}$ and

sAMOTA metrics, respectively. SFANet also improves the performance by 0.69% in $AP_{mod.}$ and 0.47% in sAMOTA by aggregating adjacent feature maps over time. Combining all the ideas, the proposed method improves $AP_{mod.}$ performance by 1.64% and sAMOTA performance by 4.34% over the baseline, which appears to be substantial.

Table 4 analyzes the performance gains achieved by the rule-based edge pruning and attention-based edge gating. We evaluate the performance gains achieved by adding each idea to a fully-connected GNN. The rule-based edge pruning offers a 1.48% improvement in sAMOTA by removing unnecessary connections from the fully-connected graph. The attention-based edge gating weights the GNN features according to their importance, which offers additional gain of 0.88% in sAMOTA. Totally, the combination of the two increases sAMOTA by 2.36% over the baseline GNN. We also analyze the runtime of the SG-GNN. While the rule-based pruning method reduces the computation time, the attention-based gating method increases the computation time for better performance. Overall, the SG-GNN reduces the runtime of the baseline GNN by 10%.

Conclusions

In this paper, we proposed a novel 3D JoDT method based on camera and LiDAR sensor fusion. In our framework, the detector and tracker work together to jointly optimize detection and object association tasks using spatio-temporal features. The detector enhances the object features by applying the weighted temporal feature aggregation to both the camera and LiDAR features. The detector uses the tracklet obtained by the tracker to reconfigure the initial outputs of the detector. The tracker uses the spatio-temporal features delivered by the detector for object association. We also devised the SG-GNN, which efficiently matches the objects on the spatio-temporal graph using a combination of rule-based edge pruning and attention-based edge gating. Our evaluation conducted on the KITTI and nuScenes datasets demonstrated that the 3D DetecTrack achieved a significant performance gain over the baseline and achieved state-of-the-art performance in some MOT evaluation categories.

Acknowledgements

This work was partly supported by the Institute of Information & Communications Technology Planning & Evaluation (IITP) grant funded by the Korea government (MSIT) (No. 2020-0-01373, Artificial Intelligence Graduate School Program (Hanyang University)) and the National Research Foundation of Korea (NRF) grant funded by the Korea government (MSIT) (No. 2020R1A2C2012146).

References

- Baser, E.; Balasubramanian, V.; Bhattacharyya, P.; and Czarnecki, K. 2019. Fantrack: 3D multi-object tracking with feature association network. In *IEEE Intelligent Vehicles Symposium (IV)*, 1426–1433.
- Bernardin, K.; and Stiefelwagen, R. 2008. Evaluating multiple object tracking performance: the clear mot metrics. *EURASIP Journal on Image and Video Processing*, 2008: 1–10.
- Brasó, G.; and Leal-Taixé, L. 2020. Learning a neural solver for multiple object tracking. In *Proceedings of the IEEE/CVF Conference on Computer Vision and Pattern Recognition (CVPR)*, 6247–6257.
- Caesar, H.; Bankiti, V.; Lang, A. H.; Vora, S.; Liong, V. E.; Xu, Q.; Krishnan, A.; Pan, Y.; Baldan, G.; and Beijbom, O. 2020. Nuscenes: A multimodal dataset for autonomous driving. In *Proceedings of the IEEE/CVF conference on Computer Vision and Pattern Recognition (CVPR)*, 11621–11631.
- Chiu, H.-k.; Prioletti, A.; Li, J.; and Bohg, J. 2020. Probabilistic 3D multi-object tracking for autonomous driving. *arXiv preprint arXiv:2001.05673*.
- Geiger, A.; Lenz, P.; and Urtasun, R. 2012. Are we ready for autonomous driving? the KITTI vision benchmark suite. In *Proceedings of the IEEE/CVF conference on Computer Vision and Pattern Recognition (CVPR)*, 3354–3361.
- Hu, H.-N.; Cai, Q.-Z.; Wang, D.; Lin, J.; Sun, M.; Krahenbuhl, P.; Darrell, T.; and Yu, F. 2019. Joint monocular 3D vehicle detection and tracking. In *Proceedings of the IEEE/CVF International Conference on Computer Vision (ICCV)*, 5390–5399.
- Ke, B.; Zheng, H.; Chen, L.; Yan, Z.; and Li, Y. 2019. Multi-object tracking by joint detection and identification learning. *Neural Processing Letters*, 50(1): 283–296.
- Kieritz, H.; Hubner, W.; and Arens, M. 2018. Joint detection and online multi-object tracking. In *Proceedings of the IEEE/CVF Conference on Computer Vision and Pattern Recognition Workshops (CVPRW)*, 1459–1467.
- Kim, H.-U.; and Kim, C.-S. 2016. CDT: Cooperative detection and tracking for tracing multiple objects in video sequences. In *Proceedings of the European Conference on Computer Vision (ECCV)*, 851–867.
- Kingma, D. P.; and Ba, J. 2014. Adam: A method for stochastic optimization. *arXiv preprint arXiv:1412.6980*.
- Kuhn, H. W. 1955. The Hungarian method for the assignment problem. *Naval research logistics quarterly*, 2(1-2): 83–97.
- Lang, A. H.; Vora, S.; Caesar, H.; Zhou, L.; Yang, J.; and Beijbom, O. 2019. PointPillars: Fast encoders for object detection from point clouds. In *Proceedings of the IEEE/CVF conference on Computer Vision and Pattern Recognition (CVPR)*, 12697–12705.
- Liang, M.; Yang, B.; Chen, Y.; Hu, R.; and Urtasun, R. 2019. Multi-task multi-sensor fusion for 3D object detection. In *Proceedings of the IEEE/CVF conference on Computer Vision and Pattern Recognition (CVPR)*, 7345–7353.
- Liang, M.; Yang, B.; Wang, S.; and Urtasun, R. 2018. Deep continuous fusion for multi-sensor 3D object detection. In *Proceedings of the European Conference on Computer Vision (ECCV)*, 641–656.
- Lin, T.-Y.; Goyal, P.; Girshick, R.; He, K.; and Dollár, P. 2017. Focal loss for dense object detection. In *Proceedings of the IEEE/CVF International Conference on Computer Vision (ICCV)*, 2980–2988.
- Lu, Z.; Rathod, V.; Votel, R.; and Huang, J. 2020. Retina-track: Online single stage joint detection and tracking. In *Proceedings of the IEEE/CVF conference on Computer Vision and Pattern Recognition (CVPR)*, 14668–14678.
- Luiten, J.; Osep, A.; Dendorfer, P.; Torr, P.; Geiger, A.; Leal-Taixé, L.; and Leibe, B. 2020. HOTA: A higher order metric for evaluating multi-object tracking. *International Journal of Computer Vision (IJCV)*, 1–31.
- Morris, C.; Ritzert, M.; Fey, M.; Hamilton, W. L.; Lenssen, J. E.; Rattan, G.; and Grohe, M. 2019. Weisfeiler and leman go neural: Higher-order graph neural networks. In *Proceedings of the AAAI Conference on Artificial Intelligence*, 4602–4609.
- Munjal, B.; Aftab, A. R.; Amin, S.; Brandlmaier, M. D.; Tombari, F.; and Galasso, F. 2020. Joint detection and tracking in videos with identification features. *Image and Vision Computing*, 100: 103932.
- Pang, S.; Morris, D.; and Radha, H. 2020. CLOCs: Camera-LiDAR object candidates fusion for 3D object detection. In *Proceedings of the IEEE/RSJ International Conference on Intelligent Robots and Systems (IROS)*, 10386–10393.
- Peng, J.; Wang, C.; Wan, F.; Wu, Y.; Wang, Y.; Tai, Y.; Wang, C.; Li, J.; Huang, F.; and Fu, Y. 2020. Chained-tracker: Chaining paired attentive regression results for end-to-end joint multiple-object detection and tracking. In *Proceedings of the European Conference on Computer Vision (ECCV)*, 145–161.
- Qi, C. R.; Su, H.; Mo, K.; and Guibas, L. J. 2017a. Pointnet: Deep learning on point sets for 3D classification and segmentation. In *Proceedings of the IEEE/CVF conference on Computer Vision and Pattern Recognition (CVPR)*, 652–660.
- Qi, C. R.; Yi, L.; Su, H.; and Guibas, L. J. 2017b. Pointnet++: Deep hierarchical feature learning on point sets in a metric space. In *Advances in Neural Information Processing Systems (NeurIPS)*, 5099–5108.
- Shenoi, A.; Patel, M.; Gwak, J.; Goebel, P.; Sadeghian, A.; Rezatofighi, H.; Martín-Martín, R.; and Savarese, S. 2020.

- Jrmot: A real-time 3D multi-object tracker and a new large-scale dataset. In *Proceedings of the IEEE/RSJ International Conference on Intelligent Robots and Systems (IROS)*, 10335–10342.
- Shi, S.; Wang, X.; and Li, H. 2019. PointRCNN: 3D object proposal generation and detection from point cloud. In *Proceedings of the IEEE/CVF conference on Computer Vision and Pattern Recognition (CVPR)*, 770–779.
- Shi, S.; Wang, Z.; Wang, X.; and Li, H. 2019. Part-A2 Net: 3D part-aware and aggregation neural network for object detection from point cloud. *arXiv preprint arXiv:1907.03670*.
- Voigtlaender, P.; Krause, M.; Osep, A.; Luiten, J.; Sekar, B. B. G.; Geiger, A.; and Leibe, B. 2019. MOTs: Multi-object tracking and segmentation. In *Proceedings of the IEEE/CVF Conference on Computer Vision and Pattern Recognition (CVPR)*, 7942–7951.
- Wang, Y.; Kitani, K.; and Weng, X. 2020. Joint object detection and multi-object tracking with graph neural networks. *arXiv preprint arXiv:2006.13164*, 5.
- Wang, Z.; Zheng, L.; Liu, Y.; Li, Y.; and Wang, S. 2020. Towards real-time multi-object tracking. In *Proceedings of the European Conference on Computer Vision (ECCV)*, 107–122.
- Weng, X.; Wang, J.; Held, D.; and Kitani, K. 2020a. 3D multi-object tracking: A baseline and new evaluation metrics. In *Proceedings of the IEEE/RSJ International Conference on Intelligent Robots and Systems (IROS)*, 10359–10366.
- Weng, X.; Wang, Y.; Man, Y.; and Kitani, K. M. 2020b. GNN3MOT: Graph neural network for 3d multi-object tracking with 2D-3D multi-feature learning. In *Proceedings of the IEEE/CVF Conference on Computer Vision and Pattern Recognition (CVPR)*, 6499–6508.
- Weng, X.; Yuan, Y.; and Kitani, K. 2020. Joint 3D tracking and forecasting with graph neural network and diversity sampling. *arXiv preprint arXiv:2003.07847*.
- Wu, H.; Li, Q.; Wen, C.; Li, X.; Fan, X.; and Wang, C. 2021. Tracklet proposal network for multi-object tracking on point clouds. In *Proceedings of the International Joint Conference on Artificial Intelligence (IJCAI)*, 1165–1171.
- Yan, Y.; Mao, Y.; and Li, B. 2018. Second: Sparsely embedded convolutional detection. *Sensors*, 18(10): 3337.
- Yang, Z.; Sun, Y.; Liu, S.; and Jia, J. 2020. 3DSSD: Point-based 3D single stage object detector. In *Proceedings of the IEEE/CVF conference on Computer Vision and Pattern Recognition (CVPR)*, 11040–11048.
- Yang, Z.; Sun, Y.; Liu, S.; Shen, X.; and Jia, J. 2019. STD: Sparse-to-dense 3D object detector for point cloud. In *Proceedings of the IEEE/CVF International Conference on Computer Vision (ICCV)*, 1951–1960.
- Yoo, J. H.; Kim, Y.; Kim, J.; and Choi, J. W. 2020. 3D-CVF: Generating joint camera and lidar features using cross-view spatial feature fusion for 3d object detection. In *Proceedings of the European Conference on Computer Vision (ECCV)*, 720–736.
- Zhai, G.; Kong, X.; Cui, J.; Liu, Y.; and Yang, Z. 2020. FlowMOT: 3D multi-object tracking by scene flow association. *arXiv preprint arXiv:2012.07541*.
- Zhang, W.; Zhou, H.; Sun, S.; Wang, Z.; Shi, J.; and Loy, C. C. 2019. Robust multi-modality multi-object tracking. In *Proceedings of the IEEE/CVF International Conference on Computer Vision (ICCV)*, 2365–2374.
- Zhang, Y.; Wang, C.; Wang, X.; Zeng, W.; and Liu, W. 2021. Fairmot: On the fairness of detection and re-identification in multiple object tracking. *International Journal of Computer Vision (IJCV)*, 1–19.
- Zheng, W.; Tang, W.; Chen, S.; Jiang, L.; and Fu, C.-W. 2021. CIA-SSD: Confident IoU-aware single-stage object detector from point cloud. In *Proceedings of the AAAI Conference on Artificial Intelligence*, 3555–3562.
- Zhou, Y.; and Tuzel, O. 2018. Voxelnet: End-to-end learning for point cloud based 3D object detection. In *Proceedings of the IEEE/CVF conference on Computer Vision and Pattern Recognition (CVPR)*, 4490–4499.